Experimental Study of Turbulent Diffusion Flames Stabilized on a Bluff Body*
(Flame Structure)

Chang Eon LEE** and Yoshiaki ONUMA**

An experimental investigation was conducted on the structure of turbulent diffusion flames of hydrogen stabilized on a bluff body. A coaxial jet diffusion flame was formed using a cylindrical nozzle with an extremely thick rim, which works as a bluff body. In the present study, special attention was paid to the effect of combustion on the aerodynamic processes. The following results were obtained. (1) The combustion markedly enhances the penetration of the central fuel jet. (2) The laminarization phenomenon, reported in simple jet diffusion flames, was observed more conspicuously in this combustion field as well, and it was assumed to exert an important influence on the flame structure. (3) An accelerating flow field often exists in complicated flow fields with a reverse flow, where turbulence generation terms containing Reynolds normal stress become negative. This phenomenon sometimes exerts considerable effects on the turbulence behavior.

Key Words: Combustion, Turbulent Diffusion Flame, Wake, Coaxial Jet, Bluff Body, Recirculation Flow, Flame Structure, Stabilized Flame

1. Introduction

Recirculating flows are often used to stabilize flames in practical combustors. Thus, it is of great technological importance to clarify the behavior of the flame with recirculation flow and to develop a modeling technique on the basis of the experimental findings. In the present study, a turbulent diffusion flame stabilized on a bluff body was chosen as one such flame. Concerning this flame, stability, structure and flow pattern have been studied over a long period of time[1]-[3], and recently, extensive studies have been carried out at the United States Air Force Aeronautical Propulsion Laboratory[4]-[7]. However, the details of the flame structure are still not understood and the numerical simulation technique is underdeveloped[8],[9].

Since the objective of this study is the development of a modeling technique for the combustion flow with recirculation zones, and obtained experimental results are intended for use as benchmark data for model testing, the combustion flow field was desired to be as simple as possible. Thus, a coaxial jet diffusion flame was formed using a cylindrical nozzle with an extremely thick rim, which acts as a bluff body. In this first report, experimental results are presented on a typical flame and the structure and flow characteristics are examined. Special attention is paid to the effect of combustion on the aerodynamic processes.

2. Experimental Apparatus and Procedure

Figure 1 shows a schematic of the axisymmetric bluff-body combustor. A cylindrical nozzle with a thick rim was installed at the center of an annular air stream issued vertically upward from an orifice of 110 mm inside diameter. The inside and outside diameters of the nozzle are 6 mm and 43 mm, respectively. The top surface of the thick rim acts as a bluff body to stabilize flames. A mixture of hydrogen and nitrogen was used as fuel and injected parallel to the air stream. Time-averaged and fluctuating velocities, gas temperature and chemical species concentration were measured for flow fields with and without combustion. The experimental conditions are shown in Table 1.

* Received 5th October, 1992. Paper No. 91-0522 A

** Department of Energy Engineering, Toyohashi University of Technology, 1-1 Hibarigaoka, Tempaku-cho, Toyohashi 441, Japan

Time-averaged and fluctuating velocities in axial ($\bar{U}$, u') and radial ($\bar{V}$, v') directions and Reynolds shear stress ($\overline{u'v'}$) were measured with a laser Doppler velocimeter. The scattering particles were suspended in both the central fuel jet and the annular air stream. Since the air flow rate is too high to supply a sufficient number of particles, another air stream (Air 2) with dense seeding was injected from the annular slit (① in Fig. 1). The flow rate of Air 2 was regulated so as not to disturb the flow field.

Species concentrations were analyzed on the dry basis with a gas chromatograph after gas sampling with a water-cooled probe of 0.51 mm inner diameter. Concentrations on the wet basis were calculated from the dry-basis results. Since the direction and magnitude of flow velocity change drastically with location in the wake region of a bluff body, measured values vary depending on probe insertion angle and suction velocity. In this measurement, the probe was always inserted vertically, and the suction velocity was kept constant at 11 m/s. Measured values did not vary below this velocity. Concentration was measured differently according to probe insertion angle; the maximum difference was 4 mole% for H_2, but changes in profiles were scarcely observed.

The gas temperature was measured with a thermocouple (Pt-Pt/13% Rh, 0.1 mm diameter) coated with Y_2O_3-BeO. Results were not corrected for radiation loss.

3. Results and Discussion

Figure 2 shows the radial profiles of initial velocities measured 1 mm downstream from the nozzle tip. In this figure, r is the radial distance from the symmetry axis, and the hatched part indicates the nozzle rim. The profiles of time-averaged velocity $\bar{U}$ and Reynolds stresses $\overline{u'^2}$ and $\overline{u'v'}$ are characteristic of a pipe flow. Though these results were measured in a noncombustion flow field, no difference between combustion and noncombustion cases was observed.

Flow patterns formed by the bluff-body combustor are shown in Figs. 3 (a) and (b) for noncombustion and combustion flows, respectively. The ordinate

Table 1 Experimental conditions

Average velocity of surrounding air flow	23 m/s
Average velocity of fuel jet	17 m/s
Volumetric mixing ratio of fuel	$H_2/N_2 = 1/2$
Reynolds number of fuel jet	4580

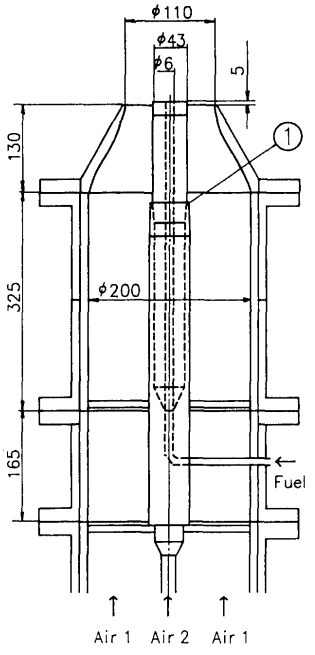

Fig. 1 Schematic of axisymmetric bluff-body combustor

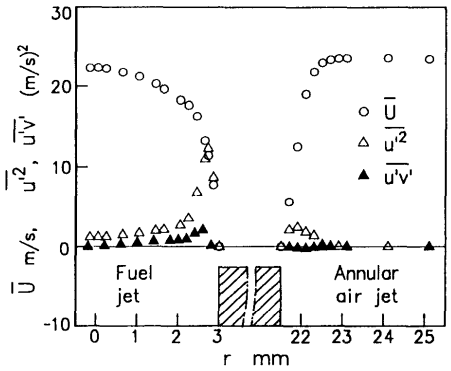

Fig. 2 Radial profiles of initial velocities

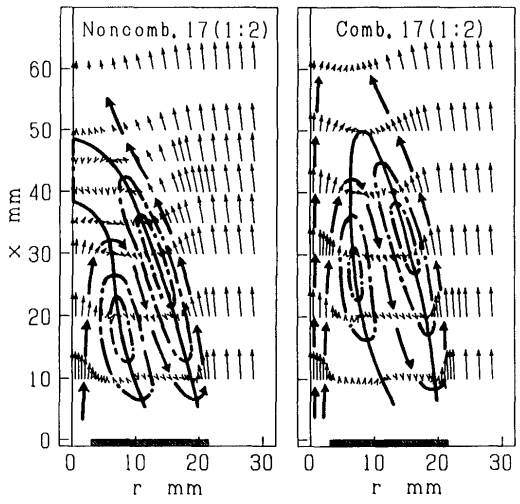

(a) Non-combustion (b) Combustion

Fig. 3 Flow patterns formed by bluff-body combustor

x represents the axial distance from the nozzle tip. Fine vector marks show the time-averaged velocity vectors obtained from measurements, and thick ones show the flow of fuel issuing from the fuel nozzle. Solid lines correspond to the location of zero time-averaged axial velocity ($\bar{U}=0$) : hence the areas within these lines are reverse-flow regions. Two counter-rotating vortices can be identified in the recirculation zone for both cases. In the noncombustion case of Fig. 3 (a), the fuel jet is reversed in the wake region, and two stagnation points in the fuel jet and air stream are observed along the centerline. This flow pattern is formed when the momentum of annular air flow dominates the flow condition, which is called an annular-air-dominated flow field. In the combustion case, the flow field is dominated by the central-jet momentum, where the fuel jet penetrates the wake region. That is, in the noncombustion case all of the fuel reverses direction through the space between the two vortices and then flows downstream with annular air, while in the combustion case, though some of the fuel follows the same path as in the noncombustion case, the rest flows directly downstream along the central axis. Comparing these two flow patterns, we see that the combustion enhances the penetration of the central jet. This may be one of the conspicuous features in combustion flow such as that shown in Fig. 3.

Figures 4 (a) and (b) show respective profiles of time-averaged axial velocity and Reynolds stress along the central axis, corresponding to Figs. 3 (a) and (b). In both figures, the time-averaged velocity decreases rapidly after the potential core and attains the minimum velocity, after which it increases with downstream distance because the central flow is accelerated by the surrounding stream. By comparing Figs. 4 (a) and (b), the phenomena wherein the potential core extends farther downstream and the fuel jet penetrates the recirculation zone can be clearly confirmed in the combustion flow field. The major causes for the increase of fuel-jet penetration have been considered to be as follows: (1) gas density around the fuel jet decreases due to high temperature, (2) negative static pressure in the wake of the bluff body is recovered due to thermal expansion. Adding to these causes, the authors propose a so-called laminarization phenomenon, wherein turbulence is suppressed due to combustion. This will be discussed later.

As for turbulence, the profiles of $\overline{u'^2}$ and $\overline{v'^2}$ have two peaks in the decelerating and accelerating regions of $\bar{U}$ in the noncombustion flow, and $\overline{u'^2}$ is larger than $\overline{v'^2}$ in the upstream peak but vice versa in the downstream peak. Such a reversal of magnitude of $\overline{u'^2}$ and $\overline{v'^2}$ is rarely seen in simple flow fields. Meanwhile, in the combustion flow, though the behavior of the upstream peak is similar to that in the noncombustion flow, the downstream peak does not appear clearly. This turbulence behavior will be examined later in terms of radial profiles of velocities.

Figure 5 shows the profiles of temperature $\bar{T}$ and chemical species concentrations along the symmetry axis. Solid and dashed lines indicate the mass fractions of hydrogen element M_H with and without combustion, respectively, and they represent concentration profiles of nozzle fluid. The region of H_2 and O_2 coexistence is located around the minimum point of $\bar{U}$ in Fig. 4 (b), which implies that the reaction zone exists in that area on the flame axis. Comparing the two M_H profiles, we find that though the nozzle fluid concentration decreases rapidly in the region above

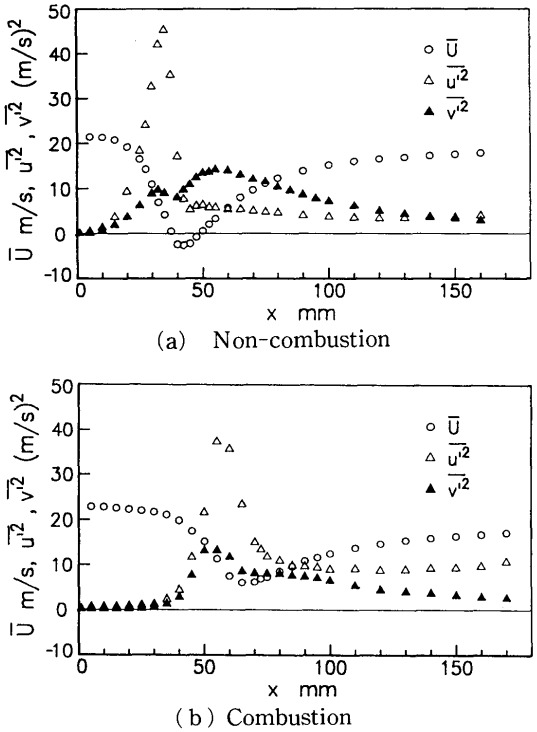

(a) Non-combustion

(b) Combustion

Fig. 4 Profiles of time-averaged axial velocity and Reynolds stresses along symmetry axis

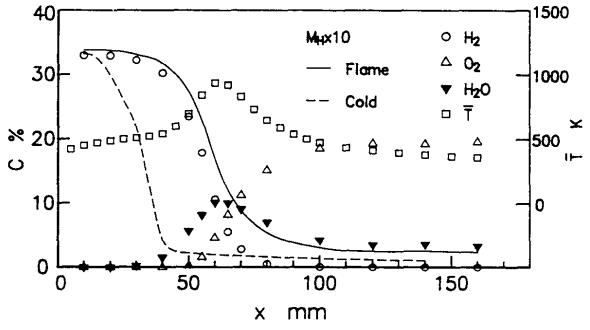

Fig. 5 Axial profiles of temperature and chemical species concentrations along symmetry axis

the stagnation point ($x=40$ mm) and becomes constant after that point in the noncombustion case, combustion lengthens the potential core of the M_H profile and decreases its dissipation rate beyond the potential core region.

Figure 6 shows the radial profiles of temperature and chemical species concentrations in several cross sections. Comparing these figures with Fig. 3 (b), we find that H_2 and O_2 coexist around the periphery of the central jet upstream and around the symmetry axis downstream, and peaks of temperature profiles are located in the coexistence regions. Namely, here combustion occurs mainly around the periphery of the central fuel jet and is nearly completed in the starting region of the reverse flow. Hence, combustion is weak in the outer recirculating vortex.

Figures 7 (a) and (b) show the radial profiles of velocities in the cross section of $x=10$ mm for noncombustion and combustion cases, respectively. All the Reynolds stresses attain their maximum values in regions where the mean velocity gradients are high; that is, in the shear layers located along the central jet boundary and along the outer boundary separating the recirculation zone and the annular air flow. However, these stresses are conspicuously suppressed throughout the cross section in the combustion case. The suppression of $\overline{u'v'}$ and $\bar{V}$ may decrease the radial diffusion rates of momentum and chemical species. This effect is evident from the fact that the radial gradient of $\bar{U}$ in the shear layer is much larger for combustion flow than for noncombustion flow. The decrease in radial momentum diffusion at the fuel jet boundary is considered to be one of the major causes of the above-mentioned phenomenon that combustion enhances the fuel jet penetration.

The suppression of turbulence mentioned above may be considered to be caused by laminarization due to combustion, which has been observed in jet diffusion flames[10]-[12]. Its mechanism may be as follows. Since a low-turbulence region attains a high temperature due to combustion, kinematic viscosity increases and the local turbulence Reynolds number decreases. As a result, the balance between generation and dissipation rates of turbulence, which is maintained in highly turbulent regions, breaks down: turbulence is then suppressed due to the dominant dissipation rate of turbulence. In jet diffusion flames, this phenomenon usually occurs in the periphery of jets, but in this bluff-body diffusion flame, it occurred in the central region of the combustion flow. Hence, it is postulated that the phenomenon may exert a larger effect on the flow field in bluff-body diffusion flames.

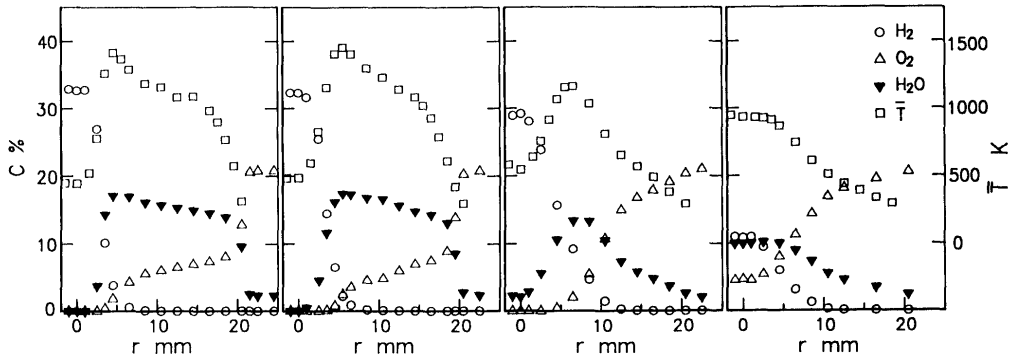

(a) $x=10$ mm (b) $x=20$ mm (c) $x=40$ mm (d) $x=60$ mm

Fig. 6 Radial profiles of temperature and chemical species concentrations in several cross sections

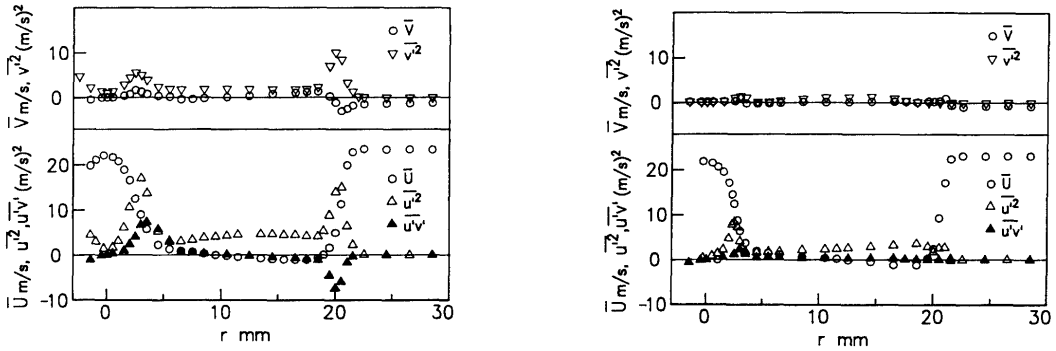

(a) Noncombustion (b) Combustion

Fig. 7 Radial profiles of velocities in the cross section of $x=10$ mm

The radial profiles of velocities in cross sections other than $x=10$ mm of Fig. 7 are shown in Figs. 8 and 9 for noncombustion and combustion cases, respectively. For both combustion and noncombustion cases, axial time-averaged velocity $\bar{U}$ has a W-shaped profile, with large values at the center and periphery in the upstream. However, in the downstream region, since the velocity of the central jet decays rapidly, the profile becomes a V-shape, as observed behind a simple bluff body in general. Figures 8 (a) and (b) and 9 (a) and (b) indicate that the positive $\bar{V}$ and $\overline{u'v'}$ contribute to the decay of the central jet. The transition point from the W-shape to the V-shape corresponds to the minimum point in the axial profile of $\bar{U}$ shown in Fig. 4, in either combustion or noncombustion cases. The momentum defect in the V-shaped profile is recovered through momentum transfer from the annular air. Figures 8 (c) and (d) and 9 (c) and (d) indicate that the transfer results from the negative $\bar{V}$ and $\overline{u'v'}$ in the shear layer.

It was pointed out in Fig. 4 (a) that the profiles of $\overline{u'^2}$ and $\overline{v'^2}$ along the symmetry axis have two peaks in the same locations, and that $\overline{v'^2}$ is larger than $\overline{u'^2}$ in the downstream peak though $\overline{u'^2}$ is larger in the upstream peak. Here, this behavior will be examined in terms of the profiles of time-averaged velocities and Reynolds stresses shown in Figs. 4 (a) and 8. The generation rates of $\bar{\rho}\overline{u'^2}$ and $\bar{\rho}\overline{v'^2}$ are given by Eqs. (1) and (2) in the cylindrical coordinate system.

$$P_u=-2\bar{\rho}\overline{u'^2}\frac{\partial\bar{U}}{\partial x}-2\bar{\rho}\overline{u'v'}\frac{\partial\bar{U}}{\partial r} \qquad (1)$$

$$P_v=-2\bar{\rho}\overline{v'^2}\frac{\partial\bar{V}}{\partial r}-2\bar{\rho}\overline{u'v'}\frac{\partial\bar{V}}{\partial x} \qquad (2)$$

First, the upstream peaks located between the two cross sections of Figs. 8 (a) and (b) will be examined. The second term on the right-hand side of Eq. (1) takes a large positive value at the central part, based on the profiles of $\bar{U}$ and $\overline{u'v'}$ shown in Figs. 8 (a) and (b), and the first term also has a positive value, as seen from Fig. 4 (a). Therefore, it

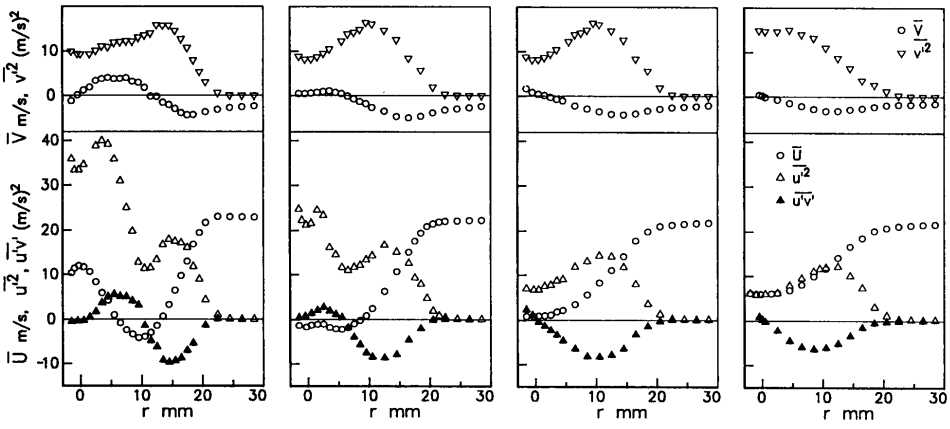

(a) $x=30$ mm (b) $x=40$ mm (c) $x=50$ mm (d) $x=60$ mm

Fig. 8 Radial profiles of velocities in several cross sections for noncombustion case

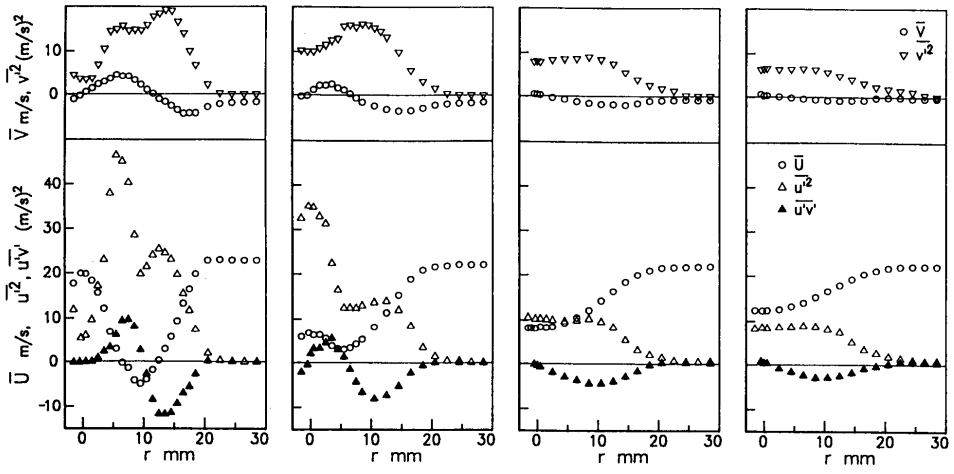

(a) $x=40$ mm (b) $x=60$ mm (c) $x=80$mm (d) $x=100$ mm

Fig. 9 Radial profiles of velocities in several cross sections for combustion case

is concluded that the $\overline{u'^2}$ generation rate P_u has a large value around the upstream peak. Meanwhile, with regard to the $\overline{v'^2}$ generation rate P_v, the first term on the right-hand side of Eq. (2) has a negative value because of the accelerating flow in the radial direction ($\partial \bar{V}/\partial r > 0$), and the second term has a small but positive value. Then, P_v should take a negative value. From the above discussion, it can be understood that $\overline{u'^2}$ is much larger than $\overline{v'^2}$ around the upstream peak and that the small peak of $\overline{v'^2}$ is formed due to not P_v but the redistribution of $\overline{u'^2}$.

Next, the downstream peaks will be examined in terms of the velocity profiles of Figs. 8 (c) and (d). The second term on the right-hand side of Eq. (1) becomes positive but small, because the value of $\partial \bar{U}/\partial r$ is small at the central part. However, the first term becomes negative because of the accelerating flow in the axial direction ($\partial \bar{U}/\partial x > 0$). Hence, P_u is considered to become negative. Meanwhile, P_v should have a positive value because, though the second term becomes nearly zero due to the small value of $\partial \bar{V}/\partial x$, the first term becomes positive due to the negative value of $\partial \bar{V}/\partial r$. As a result, the peak value of $\overline{v'^2}$ becomes larger than that of $\overline{u'^2}$ around the downstream peak. Like the upstream peak of $\overline{v'^2}$, the small peak of $\overline{u'^2}$ is thought to be formed due to the redistribution of $\overline{v'^2}$.

The behavior of $\overline{u'^2}$ and $\overline{v'^2}$ shown in Fig. 4 (a) was qualitatively explained in terms of measured results and equations for the generation rates of Reynolds normal stresses. It is observed that turbulence generation terms containing Reynolds normal stress become negative in the accelerating flow field, and that this phenomenon may exert a considerable effect on the turbulence behavior in recirculating flows.

In the combustion case shown in Fig. 4 (b), the formation of upstream peaks can be explained in terms of Figs. 9 (a) and (b), in the same manner as the noncombustion case. However, the downstream peaks are smaller than in the noncombustion case, because the values of $\partial \bar{V}/\partial r$, which contributes to the generation of $\overline{v'^2}$ in the noncombustion case, are small in the combustion case, as shown in Figs. 9 (c) and (d).

4. Conclusions

The present series of studies have been conducted in order to develop the modeling technique of turbulent diffusion flames with recirculation flow, by clarifying the flame structure experimentally and attempting a numerical simulation. In this first study, an experimental investigation was carried out on hydrogen diffusion flames stabilized on a bluff body. A coaxial jet flame was formed using a cylindrical nozzle with an extremely thick rim, which acts as a bluff body. Special attention was paid to the effect of combustion on the aerodynamic processes. The following results were obtained.

(1) The combustion markedly enhances the penetration of the central fuel jet.

(2) The laminarization phenomenon, reported in simple jet diffusion flames, was observed more conspicuously in this combustion field as well, and it was determined to exert an important influence on the flame structure.

(3) An accelerating flow field often exists in complicated flow fields with a reverse flow, where turbulence generation terms containing Reynolds normal stress become negative. This phenomenon sometimes exerts considerable effects on the turbulence behavior.

The measured results obtained in this experiment are expected to be useful as benchmark data for the modeling of turbulent diffusion flames with recirculation flow.

References

(1) Li, X. and Tankin, R.S., A Study of Cold Flow Around Bluff-Body Combustors, Combust. Sci. Tech., Vol. 52, No. 4 (1987), p. 173.

(2) Masri, A.R. and Bilger, R.W., Turbulent Diffusion Flames of Hydrocarbon Fuels Stabilized on a Bluff Body, Proc. 20th Symp. (Int.) Combust., (1984), p. 319.

(3) Kimoto, K., Shiraishi, I. and Matsumoto, R., Structure of Turbulent Jet Flames Stabilized in Annular Air Jet, Combust. Sci. Tech., Vol. 25, No. 1 (1981), p. 31.

(4) Roquemore, W.M., Britton, R.L. and Sandhu, S.S., Dynamic Behavior of a Bluff-Body Diffusion Flame, AIAA J., Vol. 21, No. 10 (1983), p. 1410.

(5) Schefer, R.W., Namanzian, M. and Kelly, J., Velocity Measurements in a Turbulent Nonpremixed Bluff-Body Stabilized Flame, Combust. Sci. Tech., Vol. 56, No. 4 (1987), p. 101.

(6) Switzer, G.L., Goss, L.P., Trump, D.D., Reevers, C. M., Stuturd, J.S., Bradley, R.P. and Roquemore, W.M., CARS Measurements in the Near-Wake Region of an Axisymmetric Bluff-Body Combustor, AIAA J., Vol. 24, No. 7 (1986), p. 1155.

(7) Namanzian, M., Kelly J.T. and Schefer, R.W., Near-Field Instantaneous Flame and Fuel Concentration Structures, Proc. 22th Symp. (Int.) Combust., (1988), p. 627.

(8) Correa, S.M., Prediction of an Axisymmetric Combusting Flow, AIAA J., Vol. 22, No. 11 (1984), p. 1602.

(9) Scott, J.N. and Hankey, W.L., Numerical Simulation of Cold Flow in an Axisymmetric Centerbody Combustor, AIAA J., Vol. 23, No. 5 (1985), p. 641.

(10) Takagi, T., Shin, H. D. and Ishio, A., Local Laminarization in Turbulent Diffusion Flames, Combust. Flame, Vol. 37, No. 2 (1980), p. 163.
(11) Takahashi, F., Mizomoto, M. and Ikai, S., Transition from Laminar to Turbulent Free Jet Diffusion Flames, Combust. Flame, Vol. 48, No. 1 (1982), p. 85.
(12) Lee, Y.J., Hayashi, T. and Onuma, Y., The behavior of Turbulence in Hydrogen Jet Diffusion Flames and Isothemal Hot Air Jets, Trans. Jpn. Soc. Mech. Eng., (in Japanese), Vol. 56, No. 528, B (1990), p. 2503.